Supplementary Information

Nanosheets of triple hydroxide/ oxyhydroxides of nickel, cobalt and manganese as an efficient electrode material for asymmetrical supercapacitor

*Anish Reghu Nath[a], Aswathi Jayachandran[b], Neelakandapillai Sandhyarani[a]**

a. Nanoscience Research Laboratory, School of Nano Science and Technology, National Institute of Technology Calicut, Calicut, Kerala, India

b. CHRIST (Deemed to be University), Hosur Road, Bengaluru, Karnataka, India

* Corresponding author: Email: sandhya@nitc.ac.in, Phone: +91 495 228 6537

Electrodeposition of nickel (N), nickel cobalt (NC) and nickel cobalt manganese (NCM)

Potentiodynamic electrodeposition of nickel (N), nickel cobalt (NC) and nickel cobalt manganese hydroxide/ oxyhydroxide (NCM) was carried out in the potential range -1.2V to 0.4V at a scan rate of 30 mV/s for 40cyles. The deposition CV plots are shown below (Figure S1).

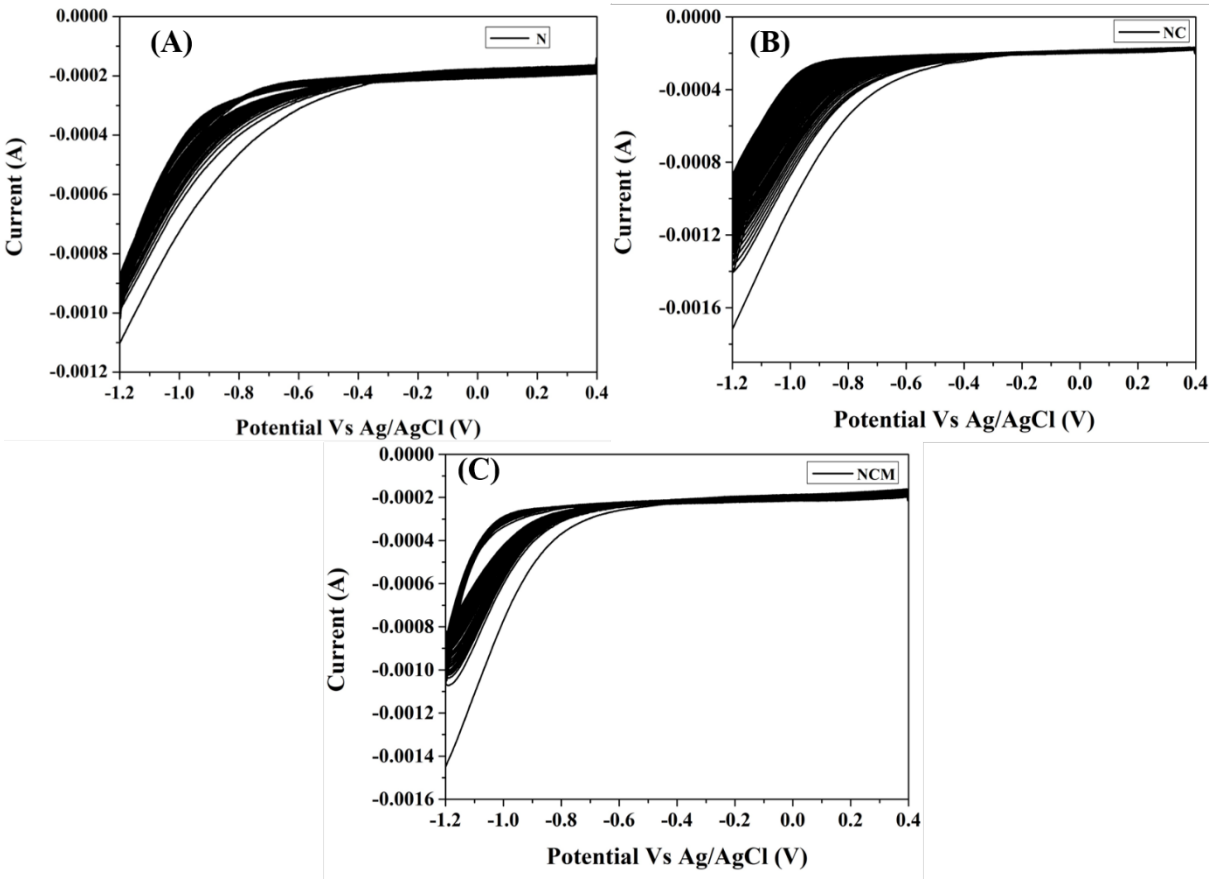

Figure S1. Electrodeposition CV curves of hydroxides/ oxyhydroxide of (A) Nickel (N) on CC (B) Nickel Cobalt (NC) on CC (C) Nickel Cobalt Manganese (NCM) on CC.

Section 1S.

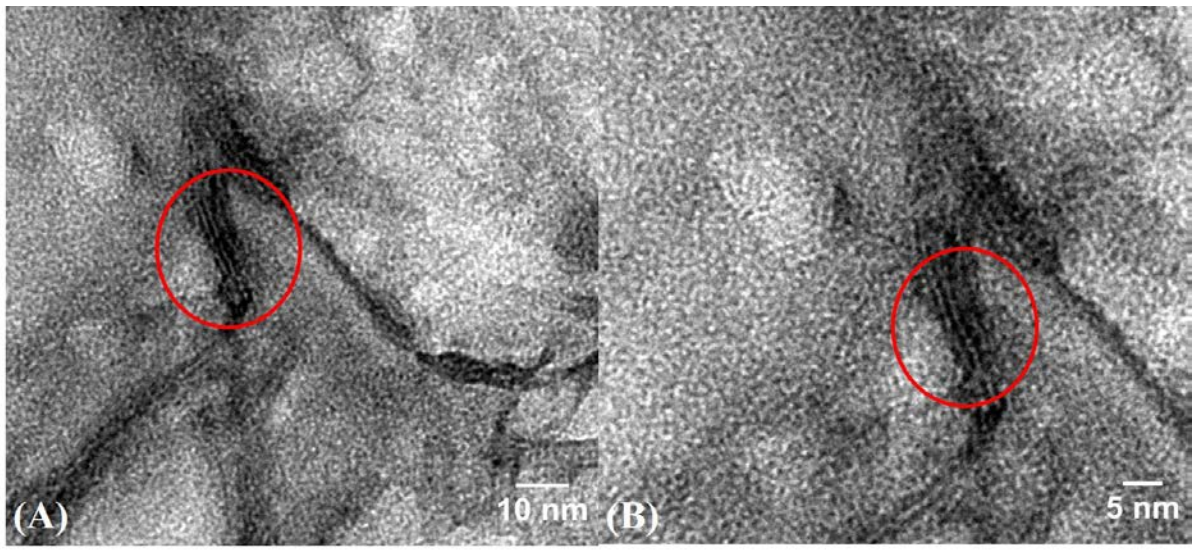

Figure S2. NCM composite electrodeposited on CC. (A, B) TEM images at different magnifications of the NCM electrode.

The TEM image of the NCM electrode, Figure S2 showing the layered morphology of the composite, shown as encircled.

The detailed XPS spectral analysis is as follows. Peaks at 642.15 eV and 653.85 eV correspond to Mn $2p_{3/2}$ and Mn $2p_{1/2}$ spin-orbit doublets of Mn 2p with spin-orbital splitting energy of 11.7eV [1,2]. Also peaks at 638.45 eV and 649.35 eV corresponds to Mn $2p_{3/2}$ and Mn $2p_{1/2}$ [3].

A prominent peak at 642.65 eV corresponds to Mn(III) [4,5] and 641.05 eV corresponding to Mn(III) ions in MnO(OH) and 643.65eV corresponds to Mn^{4+} ions and the peak at 653.85 also supports the presence of MnO(OH) [3]. Apart from the prominent existence of MnO(OH), there even exists Mn ions as Mn(II), Mn(III) and Mn(IV). Peaks confirm Mn(IV) at 646.05 eV and 644.65 eV which shows the presence of MnO_2. Mn(II) ions as MnO indicated by the peaks at 639.85 eV, 647.35 eV. A satellite peak at 648.55 eV suggests the presence of MnO at 6 eV higher binding energy concerning the Mn $2p_{3/2}$ line.

Co 2p spectrum shows two prominent peaks of Co $2p_{3/2}$ and Co $2p_{1/2}$ at 782.05 eV and 797.75 eV leaving a constant spin-orbital splitting energy [6–8]. These peaks are associated with the presence of Co^{2+} ions in CoOH. Peaks at 783.55 eV and 799.05 eV [9] corresponds to Co $2p_{3/2}$ and Co $2p_{1/2}$ of CoO(OH) [9–11] confirming the presence of Co^{3+} ions. The appearance of 1st satellite peak [12] at 3.5–6.5 eV above the Co $2p_{3/2}$ peak that is above 779.5 eV is characteristic of Co^{2+} ions evident by satellite peak at 785.35 eV. These peaks contributes to the hydroxide and oxyhydroxide of cobalt [11,13]. Peak's at 779.5 eV along with a peak at 786.75 eV corresponds to presence of Co^{3+} ions in CoO(OH) [10,11,14] and CoO respectively. Peak at 801.65 eV shows a satellite shake up peaks [15].

The Ni 2p spectrum provides two spin-orbit doublets at 856.45 eV (Ni $2p_{3/2}$) and 874.15 eV (Ni $2p_{1/2}$) leaving a constant spin-orbital splitting energy of 17.70 eV with their respective shake-up satellites [13,16]. The prominent peak at 856.45 eV, 874.15 eV, 880.15 eV corresponds to Ni^{2+} along with peaks at 857.25 eV, 875.45 eV corresponds to Ni^{3+} which shows the presence of $Ni(OH)_2$ / NiO(OH) [4,7,8,13,17–19]. Peaks at 862.95 eV shows the presence of NiO [20] while 881.45 eV could be assigned to their corresponding shake-up satellite lines [21,22]. 851.65 eV [23] and 872.45 eV shows the presence of Ni-Ni bond and presence of NiO/ $Ni(OH)_2$ [22]. The peak at 878.65 eV occurs due to the multiple splitting of energy levels [24] which is observed in Ni-containing oxides.

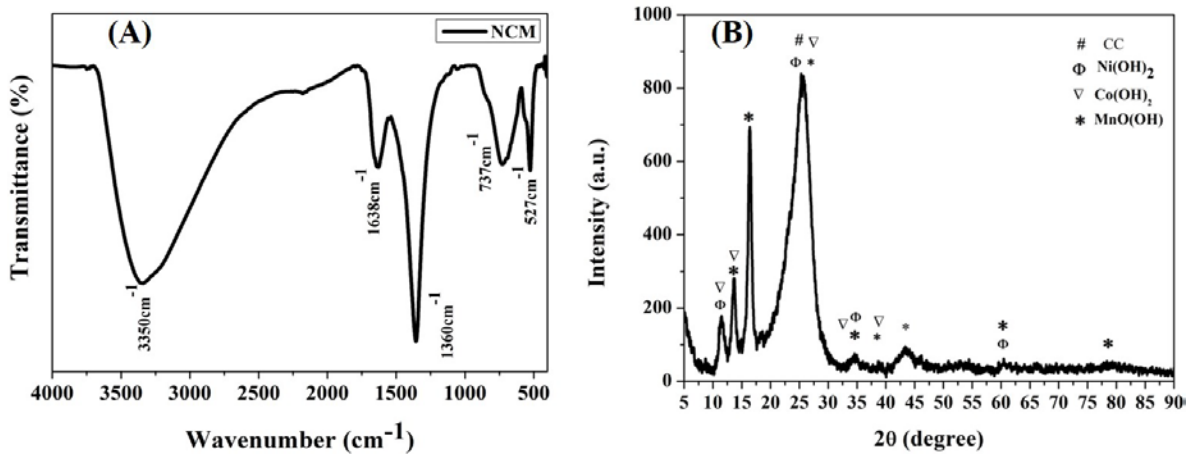

Figure S3. (A) FTIR spectrum of NCM in the presence of urea (B) XRD pattern of NCM (# -CC, *, ∇, φ ,# - hydroxides/oxyhydroxides of NCM).

Peaks at 800-600 cm^{-1} corresponds to M-O stretching vibrations and 600-400 cm^{-1} corresponds to M-OH bending vibrations[25,26].

Section 2S.

In case of N, cobalt (C) or manganese (M) electrode preparation their respective nitrate was used along with 0.8M urea in aqueous medium, mixed under sonication. Whereas during the preparation of NC both nickel and cobalt nitrates were used along with urea. A carbon cloth of 2 cm^2 was used for deposition with an electrodeposited area of 1cm^2. The samples of NC were electrochemically tested in different concentrations of nickel to cobalt. The N electrode sample is electrochemically tested as shown in (Figure S4 A & B), the C electrode sample is electrochemically tested as shown in (Figure S4 C & D) and the M electrode sample is electrochemically tested as shown in (Figure S4 E & F). Varying molar ratio of 1: 1, 1:2 and 2:1 as to nickel to cobalt denoted as 1NC1 (Figure S5 A & B), 1NC2 (Figure S5 C & D) and 2NC1 (Figure S5 E & F) electrodes respectively.

The electrochemical influence of single hydroxide electrodes nickel (N), cobalt (C) and manganese (M) and double hydroxide electrodes nickel-cobalt (NC) over nickel cobalt manganese (NCM) was studied under similar environmental conditions.

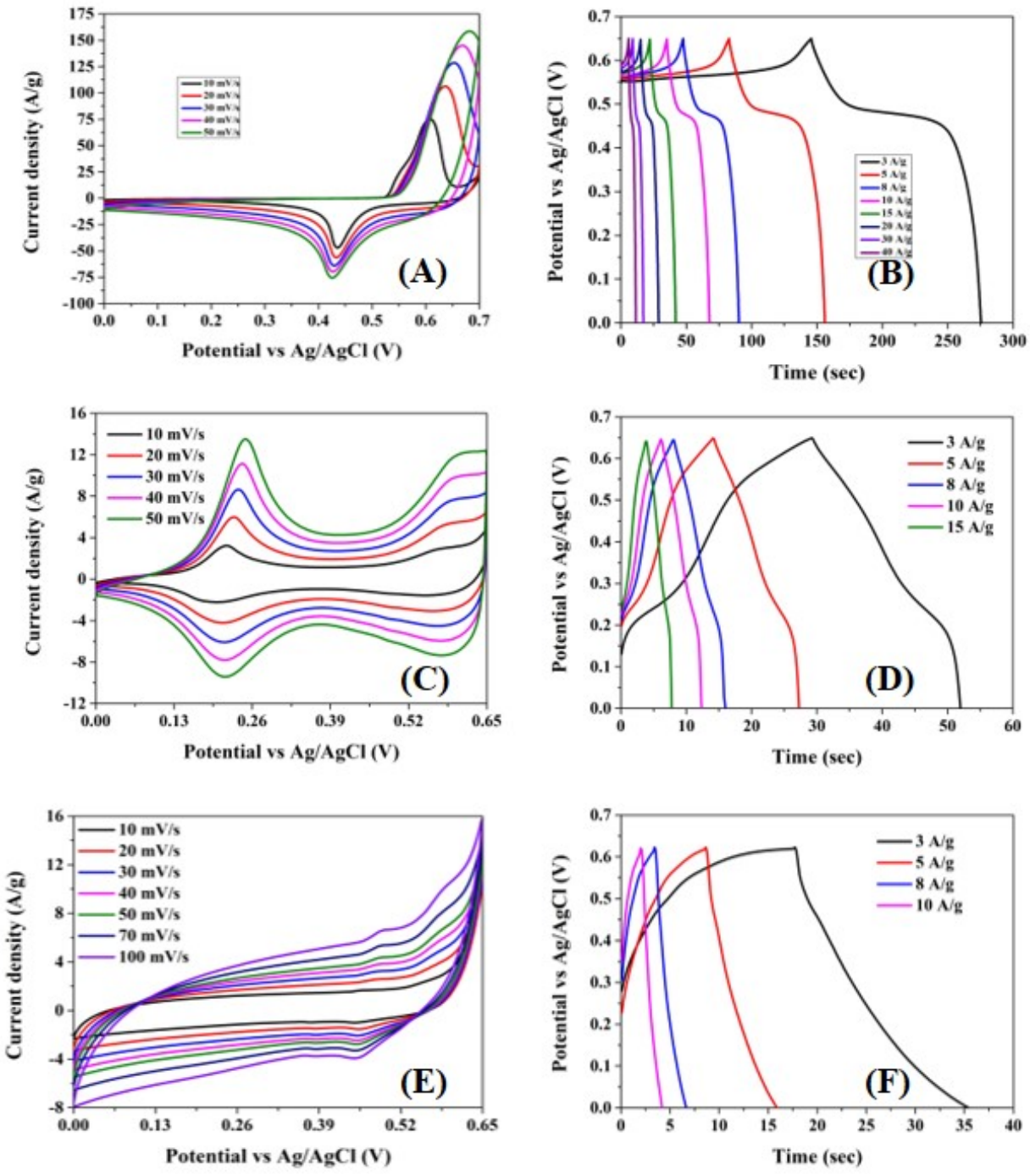

Figure S4. (A) Cyclic voltammogram of N electrode on CC, (B) Charge-discharge characteristics of N electrode on CC, (C) Cyclic voltammogram of C electrode on CC, (D) Charge-discharge characteristics of C electrode on CC, (E) Cyclic voltammogram of M electrode on CC, (F) Charge-discharge characteristics of M electrode on CC.

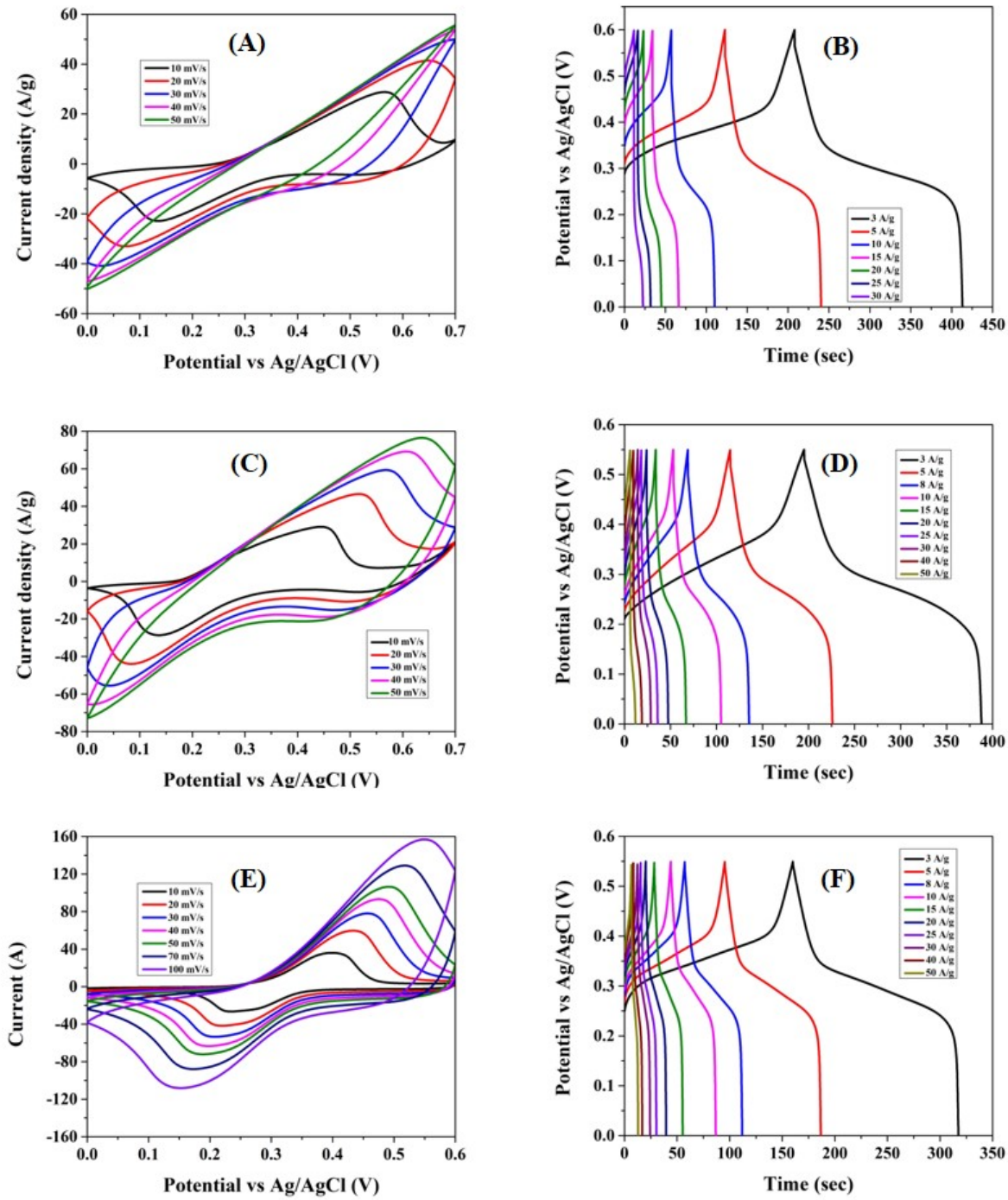

Figure S5. (A) Cyclic voltammogram of NC 1:1 ratio at different scan rates and (B) charge-discharge curves of NC 1:1 ratio at different current densities (C) Cyclic voltammogram of NC 1:2 ratios at different scan rates and (D) charge-discharge curves of NC 1:2 ratios at different current densities (E) Cyclic voltammogram of the NC 2:1 ratio at different scan rates and, (F) charge-discharge curves of NC 2:1 ratio at different current densities.

As shown in Figure S4 (A & B), the nickel (N) delivered a specific capacitance of 600F/g (108 C/g) at 3A/g in a voltage window of 0.65V without any IR drops.

An efficient electrode should have specific capacitance as well as a wider potential window with no obvious IR drop. In order to achieve this, we introduced cobalt into the electrode as in case of 1NC1, 1NC2 and 2NC1 samples. As seen in Figure S5 (A & B), the introduction of cobalt has indeed increased the specific capacitance to 1000 F/g at 3 A/g (167 C/g) but with a limited voltage window of 0.6 V compared to N sample. The cobalt concentration was further increased to 1NC2 as in Figure S5 (C & D) but resulted in a prominent IR drop. The 1NC2 sample was able to provide a specific capacitance of 1050 F/g at 3 A/g (160.5 C/g) at a potential window of 0.55 V. The increase in specific capacitance is more likely to the lower potential window as the specific capacitance is inversely proportional to voltage window. As shown in Figure S5 (E & F), the cobalt concentration was not further increased as it had adverse effect like the IR drop and hence the nickel concentration was further increased to achieve 2NC1 sample. 2NC1 has been able to deliver a specific capacitance of 850 F/g at 3 A/g (131 C/g) with no IR drop but with a limited potential window of 0.55 V. So, in order to achieve an electrode which can deliver both specific capacitance and voltage window manganese was introduced to the 2NC1 sample which had no IR drop. This introduction of manganese proved to increase the potential window to 0.7 V with no obvious IR drop.

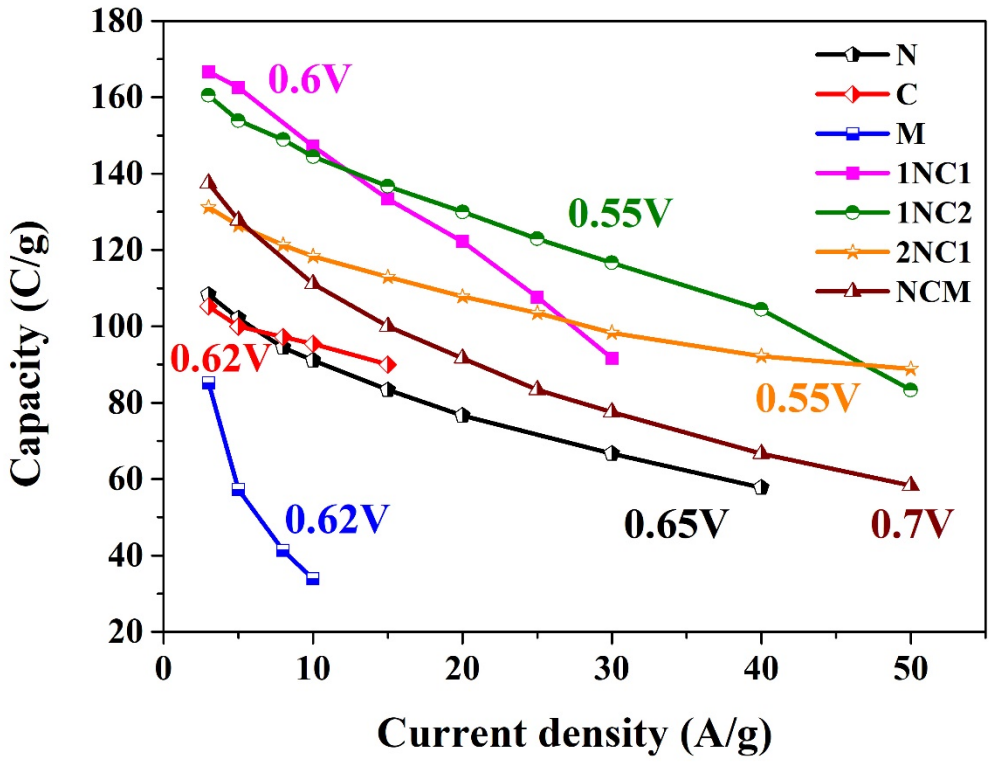

Figure S6. Capacity of different electrodes N, C, M, 1NC1, 1NC2, 2NC1 and NCM with respect to different current densities are plotted with corresponding voltage window.

As shown in Figure S6, the capacity of different electrodes N, C, M, 1NC1, 1NC2, 2NC1 and NCM electrodes are studied with their respective voltage window with varying current

densities. NCM showed a better performance considering the wide potential window and absence of IR drop and better capacity as explained above.

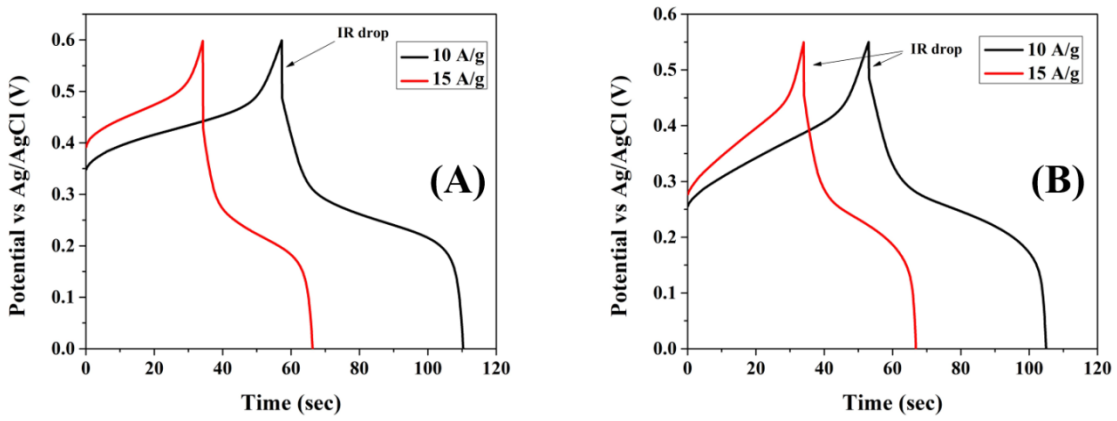

Figure S7. (A) Charge-discharge curves of NC 1:1 ratio at different current densities of 10 A/g and 15 A/g, (B) Charge-discharge curves of NC 1:2 ratios at different current densities of 10 A/g and 15 A/g.

As seen in Figure S7 (A & B), there is obvious IR drop in both these samples hence the actual potential window of 1NC1 and 1NC2 are 0.48 V rather than 0.6 V and 0.55V (considering IR drop).

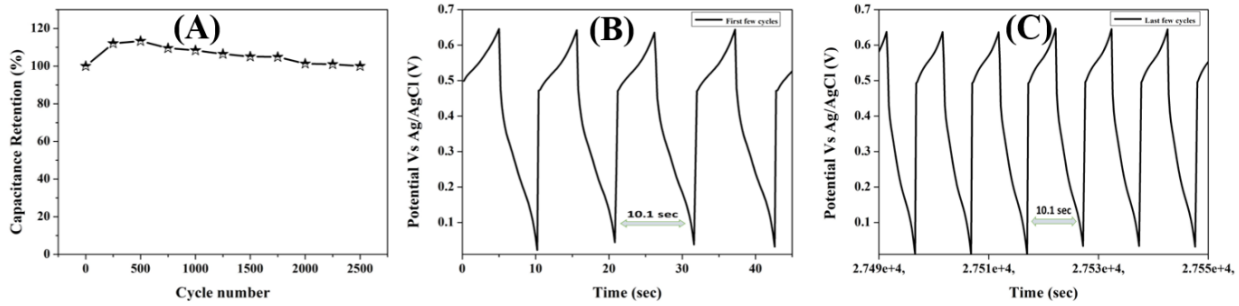

Figure S8. (A) Cyclic stability of NCM for 2500 cycles (B) cyclic stability during the first few cycles (C) cyclic stability during the last few cycles in 3M KOH electrolyte solution.

Figure S8 (A), shows a steady increase in capacitance in the initial periods of the cyclic stability test, till 500cycles. Towards the end of 2500cycles, the capacitance value achieved a stability and this was maintanined towards the end of 2500 cycles. Figure S8 (B) & (C) shows

the stability at first 5 cycles and last 5 cycles of the 2500cycles. The NCM electrode showed a capacitive retention of 100% even after 2500 cycles which showed the stability of the electrode.

Section 3S

Electrochemical studies of AC

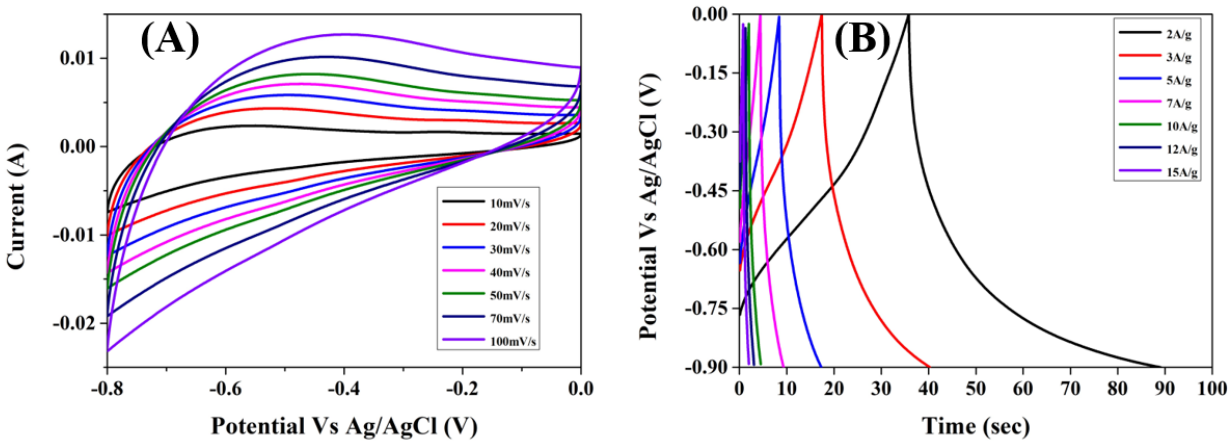

Figure S9. (A) Cyclic voltammogram of AC at different scan rates and (B) charge-discharge curves of AC at different current densities.

The cyclic voltammetry and charge discharge performance of activated carbon was studied as shown in Figure S9. The Figure S9 (A) shows the cyclic voltammogram of AC at a scan rate ranging from 10 to 100 mV/s in 3 M KOH as electrolyte solution. The CV curve of AC electrode shows a nearly rectangular shape without any noticeable redox peaks from 0 to -0.8V which indicates the capacitive behaviour of the electrode where the charges are stored as electric double layer charging/discharging. From the CD characteristics the specific capacitance of AC was found to be 80 F/g.

REFERENCES

1 A. N. Naveen and S. Selladurai, *RSC Adv.*, 2015, **5**, 65139–65152.

2 F. Grote, R.-S. Kühnel, A. Balducci and Y. Lei, *Appl. Phys. Lett.*, 2014, **104**, 053904.

3 D. Brune, R. Hellborg, H. J. Whitlow and O. Hunderi, *Surface Characterization*, Wiley-VCH, Scandinavian Science Publisher, Weinheim, Germany, 1997.

4 M. C. Biesinger, B. P. Payne, A. P. Grosvenor, L. W. M. Lau, A. R. Gerson and R. S. C. Smart, *Appl. Surf. Sci.*, 2011, **257**, 2717–2730.

5 E. S. Ilton, J. E. Post, P. J. Heaney, F. T. Ling and S. N. Kerisit, *Appl. Surf. Sci.*, 2016,

366, 475–485.

6 B. H. R. Suryanto, X. Lu, H. M. Chan and C. Zhao, *RSC Adv.*, 2013, **3**, 20936.

7 L.-K. Wu, W.-Y. Wu, J. Xia, H.-Z. Cao, G.-Y. Hou, Y.-P. Tang and G.-Q. Zheng, *J. Mater. Chem. A*, 2017, **5**, 10669–10677.

8 H. Cheng, Y. Su, P. Kuang, G. Chen and Z. Liu, *J. Mater. Chem. A*, 2015, **3**, 19314–19321.

9 J. Qi, W. Zhang and R. Cao, *Chem. Commun.*, 2017, **53**, 9277–9280.

10 J. W. Murray and J. G. Dillard, *Geochim. Cosmochim. Acta*, 1979, **43**, 781–787.

11 J. Yang, H. Liu, W. N. Martens and R. L. Frost, *J. Phys. Chem. C*, 2010, **114**, 111–119.

12 A. N. Naveen and S. Selladurai, *RSC Adv.*, 2015, **5**, 65139–65152.

13 A. Pendashteh, J. Palma, M. Anderson and R. Marcilla, *RSC Adv.*, 2016, **6**, 28970–28980.

14 B. Uthaman, K. S. Anand, R. K. Rajan, H. H. Kyaw, S. Thomas, S. Al-Harthi, K. G. Suresh and M. R. Varma, *RSC Adv.*, 2015, **5**, 86144–86155.

15 J. Ye, W. Chen, S. Xu, Z. Yu and S. Hou, *RSC Adv.*, 2016, **6**, 104925–104932.

16 M. Zhang, X. Ma, H. Bi, X. Zhao, C. Wang, J. Zhang, Y. Li and R. Che, *J. Colloid Interface Sci.*, 2017, **502**, 33–43.

17 W. Xu, H. Zhang, G. Li and Z. Wu, *Sci. Rep.*, 2015, **4**, 5863.

18 L. M. Moroney, R. S. C. Smart and M. W. Roberts, *J. Chem. Soc. Faraday Trans. 1 Phys. Chem. Condens. Phases*, 1983, **79**, 1769.

19 M. C. Biesinger, B. P. Payne, L. W. M. Lau, A. Gerson and R. S. C. Smart, *Surf. Interface Anal.*, 2009, **41**, 324–332.

20 P. Ganesan, A. Sivanantham and S. Shanmugam, *J. Mater. Chem. A*, 2016, **4**, 16394–16402.

21 P. R. Chowdhury and K. G. Bhattacharyya, *Photochem. Photobiol. Sci.*, 2017, **16**, 835–839.

22 N. Srivastava, T. Shripathi and P. C. Srivastava, *J. Electron Spectros. Relat. Phenomena*, 2013, **191**, 20–26.

23 J. Soo Kang, M.-A. Park, J.-Y. Kim, S. Ha Park, D. Young Chung, S.-H. Yu, J. Kim, J. Park, J.-W. Choi, K. Jae Lee, J. Jeong, M. Jae Ko, K.-S. Ahn and Y.-E. Sung, *Sci. Rep.*, 2015, **5**, 10450.

24 X. Jiang, Y. Sha, R. Cai and Z. Shao, *J. Mater. Chem. A*, 2015, **3**, 10536–10544.

25 X. Wang and L. Andrews, *J. Phys. Chem. A*, 2006, **110**, 10035–10045.

26 D. A. Köse and H. Necefoğlu, *J. Therm. Anal. Calorim.*, 2008, **93**, 509–514.